Influence of nanosilica and binary oxide systems on the selected physical and mechanical properties of cement composites

Agnieszka Ślosarczyk [1], Izabela Klapiszewska [1], Łukasz Klapiszewski [2]

[1] Institute of Building Engineering, Faculty of Civil and Transport Engineering, Poznan University of Technology, Piotrowo 3, PL-60965 Poznan, Poland

[2] Institute of Chemical Technology and Engineering, Faculty of Chemical Technology, Poznan University of Technology, Berdychowo 4, PL-60965 Poznan, Poland

Corresponding authors: agnieszka.slosarczyk@put.poznan.pl, lukasz.klapiszewski@put.poznan.pl

Abstract: The paper presents the results of physical and mechanical tests of cement composites that include small amounts of nanosilica, as well as systems of nanosilica with less commonly used iron and nickel nanooxides. In the work, a physicochemical analysis of the nanooxides was performed to compare their morphological and structural properties, to determine their temperature stability and to assess their behavior in the cement matrix environment. Particle distribution analysis indicated a tendency for nanooxide particles to aggregate and agglomerate, with nickel nanooxide showing the highest degree of homogeneity. For iron nanooxide, the largest size scatter and the largest particle aggregates were observed. As expected, the nanosilica displayed the highest specific surface area, whereas, both nickel and iron nanooxide exhibited higher electrokinetic and temperature stability compared to nanosilica, which guarantees their durability in high pH cement matrixes. Cement composites with oxide additions had slightly lower density and comparable absorbability after 28 days of curing, as compared to pure mortar. In the case of nanosilica, after 7 days of curing, a significant increase in compressive strength was observed in comparison with pure mortar, while the strengths were slightly lower at a later time. Synergistic application of nanosilica with nickel or iron nanooxide resulted in significant increases in strength after 28 and 90 days of curing, where the effect of nanosilica alone was not as spectacular.

Keywords: cement composites, nanosilica, binary oxides

1. Introduction

The first document that clearly describes the potential of nanotechnology in construction and building materials is the RILEM Technical Committee 197-NCM "Nanotechnology in Construction Materials" report. It covers e.g. the usage of nanoparticles in order to increase the strength and durability of cement composites (Zhu et al., 2004). With regard to nanoparticles, various inorganic oxides have been used in concrete research, but the most common are silicon oxide, iron oxides, titanium oxide, zinc oxide and aluminium oxide (Sanchez et al., 2010). There are also studies where less common oxides of zirconium, nickel or copper were added to the cement-based composites (Negahdary et al., 2013; Ślosarczyk et al., 2017; Nazari et al., 2011). The beneficial factors of nanoparticles addition in enhancing cement composite performance can be listed: well-dispersed nanoparticles raise the viscosity of the liquid phase which leads to workability improvement; they also accelerate hydration processes, densified cement paste microstructure and improve bonding between cement paste and aggregates or fibre reinforcement; and consequently reduce the porosity of the cement paste, which in turn improves the mechanical properties and durability of the cement composite (Sobolev, 2016).

Up to now the most commonly used nanooxide in concrete is nano-SiO_2. In many reports, the use of nanosilica has proven to have a positive effect on the properties of cement composites, for the most part, by accelerating the hydration process of cement and improving the strength of final material. What is more nanosilica decreases water penetration and can lower the degradation process of concrete by

controlling calcium leaching. Worth mentioning is the fact that even small amounts of nano-SiO₂ at a level 0.25 wt.% can lead to quite notable increases of compressive and flexural strength. However, results are highly dependent on dispersion of nano-SiO₂ within the mixture. This can be affected by too high amount of nano-SiO₂ addition or its size and extensive BET surface area (Sanchez and Sobolev, 2010; Sobolev, 2016). Therefore, there are studies in which nanosilica is combined with other nanooxides, thus modifying rheological and structural properties of cement composites or giving them new functionalities, e.g. antibacterial or photocatalytic (Janczarek et al., 2021; Klapiszewska et al., 2021; Sobolev, 2016; Otulu and Şahin, 2011). The aim of this paper was to ascertain the synergic effect of small amounts of nanosilica in combination with less frequently used nickel and iron nanooxides on selected physicomechanical properties of cement composites. Additionally, physicochemical analysis of the oxides used and evaluation of the microstructure of the cement composites made with them were carried out.

2.   Materials and methods

2.1. Materials

In this study, the following substances were used as admixtures for cement mortars: silicon dioxide (particles 10-20 nm, 99.5% purity, CAS: 7631-86-9), nickel (II) oxide (nanopowder with grain size <50 nm, 99.8% purity, CAS: 1313-99-1) and iron (II, III) oxide powder (particles 50-100 nm, 97% purity, CAS: 1317-61-9). All oxides were produced by Merck (Darmstadt, Germany).

CEM I Portland cement (Górażdże Cement SA, Górażdże, Poland) and ordinary quartz sand of grain up to 1 mm in size (Kwarcmix, Tomaszów Mazowiecki, Poland) were used to make the cement mortars. The last but not least material used was superplasticizer Sika®ViscoCrete®-3 (Sika Poland Sp. z o.o., Warsaw, Poland).

2.2.   Physicochemical and dispersive properties of oxide admixtures

2.2.1. Particle size distribution

Particle size distribution analysis was examined through utilizing the Zetasizer Nano ZS apparatus (Malvern Instruments Ltd., Malvern, UK) according to the non-invasive back scattering method. This method measures particles from 0.6 to 6000 nm. As part of our work, the particle size distribution was measured in isopropanol as dissolution medium.

2.2.2. Porous structure properties

In order to determine the parameters of the porous structure, an ASAP 2020 apparatus (Micromeritics Instrument Co., Norcross, USA) physisorption analyzer was employed. This operates on the basis of low-temperature nitrogen. Surface area was established by applying the multipoint BET method, using adsorption data in a relative pressure (p/p_0) range of 0.05–0.30. The desorption isotherm was used to determine the pore size distribution based on the Barrett–Joyner–Halenda (BJH) model. Before the measurements, all materials were degassed at 120 °C for 4 h. Due to the high accuracy of the instrument used, the surface area, pore volume and pore size were determined with accuracies of 0.1 m²/g, 0.001 cm³/g and 0.01 nm, respectively.

2.2.3. Electrokinetic properties

The Zetasizer Nano ZS apparatus (Malvern Instruments Ltd., Malvern, UK) was employed to measure the zeta potential, which, through measurement of electrophoretic mobility via laser Doppler velocity (LDV), enables the calculation of the zeta potential using the Henry equation:

$$\mu_E = \frac{2\varepsilon\zeta f(\kappa a)}{3\eta} \tag{1}$$

where: μ_E – electrophoretic mobility, ε – dielectric constant, ζ – electrokinetic (zeta) potential, η – viscosity, and $f(\kappa a)$ is the Henry function. The measurement took place in the pH range from 2 to 11, in the presence of 0.001 M NaCl electrolyte, which allowed determination of the electrokinetic curves. The measurement was carried out three times and the final value is the average value. The mean standard error of the zeta potential measurement is ± 2 mV, while the pH measurement error is ± 0.1.

2.2.4. Thermal stability

A Jupiter STA449 F3 apparatus (Netsch, Selb, Germany) was used to perform the thermogravimetric analysis (TGA) and to determine the first derivative of the TGA curve - the DTG curve. As part of the tests, 10 mg of samples were placed in an Al_2O_3 crucible, and then heated in a nitrogen atmosphere, at a rate of 10 °C/min, from 30 to 1000 °C, with a gas flow rate of 40 cm³/min.

2.3. Creating cement composites with binary oxide systems

In order to obtain cement composites, 270 g of aggregate and 150 g of cement were introduced into a mixing bowl. The applied admixture of nano-SiO_2 (in the amount of 0.6% - 0.9 g) and nano-NiO or nano-Fe_3O_4 (in the amount of 1.5% - 2.25 g) was initially mixed manually with the cement and aggregate. The set volume of the plasticizer (3 mL) was taken up in water (45 mL), and in the next step, everything was transferred to the mixing bowl, followed by automatic mixing. Mixing was carried out using a Renfert Twister series automatic mixer (Renfert GmbH, Hilzingen, Germany) with a mixing speed of 350 rpm and time of 3 min. The w/c ratio for the cement mortars made was 0.3.

2.4. Cement composites tests

2.4.1. Density

The density of the obtained cement mortar samples was calculated on the basis of the mass of these samples and the volumes they occupied, in accordance with the formula (1):

$$\rho = \frac{m}{V} \tag{1}$$

where: m – mass value of sample; V – volume of sample.

2.4.2. Water absorption

Water absorption tests were performed for samples of cement mortars after 28 days of maturation. The test consisted in initial weighing of samples soaked with water, and then placing them in a laboratory dryer at 105 °C. The mass was measured every 24 h until it was stabilized. Water absorption of concrete (%) was calculated with 0.1% accuracy from the given formula (2):

$$w = \frac{G_2 - G_1}{G_1} \cdot 100\% \tag{2}$$

where: G_1 – mass value of dry samples; G_2 – mass value of saturated samples.

2.4.3. Compressive strength test

Compressive strength testing of the prepared cement mortar samples was undertaken after 7, 28 and 90 days of maturation. Cylindrical specimens with dimensions of ϕ20x21 mm were placed on an INSTRON Satec testing machine (Instron, Norwood, USA). Constant displacement of machinery plates was set at 4.8 mm per minute during testing. The whole examination process lasted until the destruction of the sample.

2.4.4. Microstructural analysis

Microstructural analysis of the obtained cement samples was carried out using the TESCAN/VEGA 3 scanning electron microscope (Tescan, Brno, Czech Republic). Herein, the structure of samples containing the analyzed admixtures was visualized and assessed.

3.   Results and discussion

3.1.   Physicochemical and dispersive properties of oxide admixtures

3.1.1. Dispersive properties

The obtained results of the dispersion analysis allowed for the determination of the particle size distribution curves, which are presented in Fig. 1.
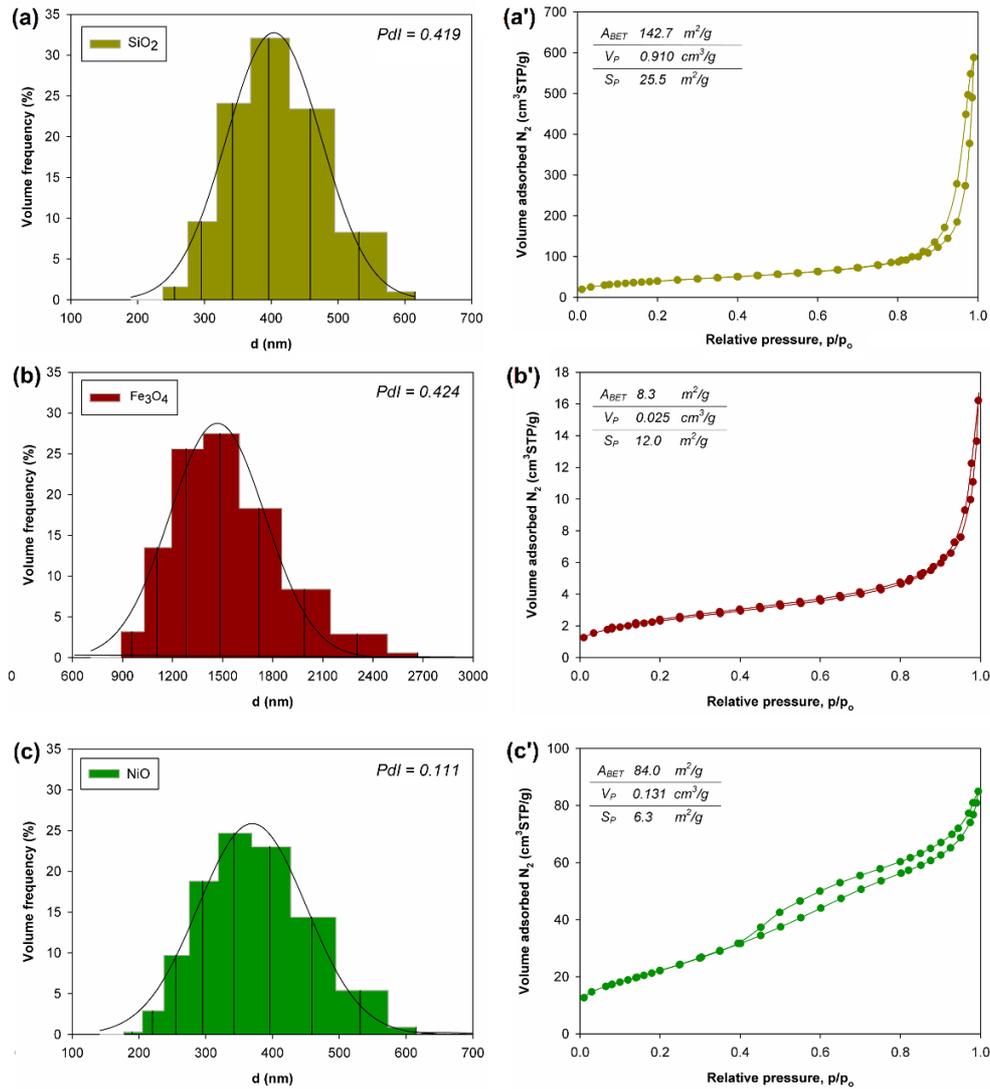
Fig. 1. Particle size distribution (a, b, c) compared with properties of porous structure and N_2 adsorption/desorption isotherms (a', b', c') of silicon dioxide (a, a'), magnetite (b, b') and nickel(II) oxide (c, c')

Fig. 1a shows the particle size distribution curve for SiO_2. On the basis of the presented diagram, it can be concluded that particles with a diameter of about 400 nm are the most numerous in the sample, while the polydispersity index (a measure of the homogeneity of the tested sample) is 0.419. In the case of the analyzed magnetite sample (see Fig. 1b), particles with significantly larger diameters in the range of 890-2700 nm were observed, but with a polydispersity index comparable to the silica sample that is equal to 0.424. In turn, in the case of the nickel (II) oxide sample (see Fig. 1c), the particle size range for the analyzed material is 189-650 nm, with the largest group of particles sized about 380 nm. The polydispersity index is 0.111 and indicates that the analyzed product has the highest homogeneity among the analyzed materials. The presented data clearly indicate the tendency of the analyzed particles to aggregate and agglomerate, which in the case of oxide systems has already been confirmed in previous studies (Bagwe et al., 2006; Zhao et al., 2008).

3.1.2. Porous structure properties

As part of the research, the most important parameters of the porous structure were also determined, including the BET surface area (A_{BET}), the total pore volume (V_p) and the average pore size (S_p). According to the obtained data (presented in Fig. 1a'-1c'), silica has the largest BET surface area at 142.7 m^2/g, whereas nickel oxide showed that this material obtains the value of 84.0 m^2/g, while the lowest A_{BET} parameter is expressed by magnetite at 8.3 m^2/g. Here, the size of the BET surface area for SiO_2 is

related to the method of its synthesis and the related morphological and microstructural properties. Silicas obtained by the sol-gel method are characterized by a relatively low specific surface, in contrast to those obtained by precipitation or high-temperature processes (Dorcheh and Abbasi, 2008; Klapiszewski et al., 2014; Krysztafkiewicz et al., 1997; Zdarta et al., 2015). When comparing the parameters related to the total pore volume, the highest value was obtained by silica (0.910 cm^3/g), followed by nickel oxide (0.131 cm^3/g), and then magnetite (0.025 cm^3/g). When comparing the mean pore size values, silica had the highest value of 25.5 nm^2/g, while nickel oxide displayed the lowest at 6.3 nm^2/g.

3.1.3. Zeta potential

Fig. 2 presents zeta potential versus pH for the oxides used in our research. In the analyzed pH range, the electrokinetic curves reach zeta potential values within the range -41.0-2.8 mV. Moreover, SiO_2 and Fe_3O_4 curves show electrokinetic stability over a pH range of 3.8 and 4.3, respectively, compared to nickel(II) oxide, for which this range starts at 5.7 pH. Only the zeta potential curve for nickel(II) oxide, which is characterized by relatively the highest potential values, reached the isoelectric point at pH = 1.8. The range of the other electrokinetic curves includes only negative potential values.
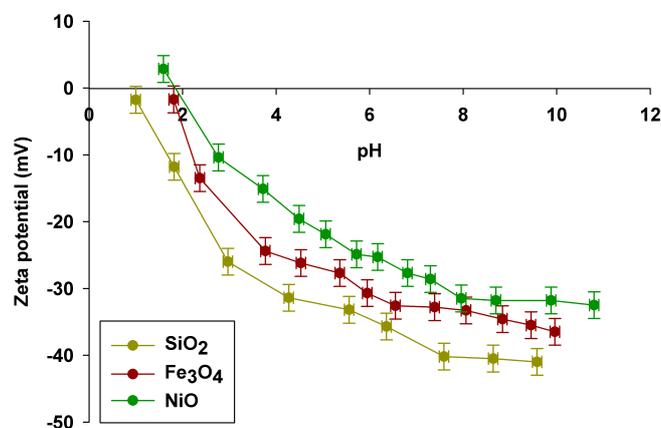

Fig. 2. Zeta potential of admixtures used in research

Similar zeta potential values for silica were obtained by the authors of the works (Song et al., 2008; Kamada et al., 2005), who presented the potential curves for the mentioned oxide characterized by electrokinetic stability starting from ~4.0 and ~3.5 pH, respectively. In the investigations of the electrokinetic stability of magnetite by Li et al. (Li et al., 2015), the pH range in which the analyzed magnetite sample shows electrokinetic stability starts at 6.2 pH. The difference between the experimentally obtained values and those presented in the literature may result from the dissociation tendency or the ionization properties of the hydroxyl groups present on the surface of the oxides (Kamada et al., 2005).

3.1.4. Thermal analysis

The data obtained from the thermogravimetric analysis for the three analyzed oxides is presented in Fig. 3. The discussed oxides are characterized by high thermal stability, as evidenced by the small mass losses of the samples. In the case of the magnetite sample, the weight loss of the sample is 0.5%, that of nickel (II) oxide is 3%, and that of silicon dioxide is 7%, respectively. The DTG SiO_2 curve (see Fig. 3b) clearly shows the effect related to the loss of sample mass (approx. 100 °C) due to the desorption of water physically bound to the oxide surface. Slight effects can also be observed with regard to the curves of the remaining oxides. Similar results for SiO_2 were also shown in the work of Klapiszewski et al. (Klapiszewski et al., 2016), where silicon dioxide was used as a component of hybrid materials based on lignin that were introduced as a filler into polymers. Comparing different mass fractions of SiO_2 to lignin, they revealed the higher thermal stability of the produced hybrid materials in relation to pristine lignin, which is undoubtedly the effect of the use of silicon dioxide. The thermogravimetric curve for

NiO was determined in work by Xavier (Xavier, 2020), who compared unmodified and modified NiO. Xavier showed that the initial weight loss occurs due to the removal of water that is surface bound to the oxide surface (temperature 50-160 °C) and can result in a weight loss of about 0.2%. The subsequent weight loss in the temperature range of 250 to 660 °C is about 1.1%. The observed mass loss effect is caused by the formation of water molecules as a result of the reaction between -OH groups on the $Ni(OH)_2$ surface. Hasan et al. (Hasan et al., 2019), in their work, presented the thermogravimetric curves for magnetite, chitosan and materials resulting from the combination of these two components. The curve for Fe_3O_4 is shown in the temperature range 30-800 °C. In the discussed article, the magnetite sample achieved a 2% weight loss due to the low moisture content of the sample. A similar weight loss of 2% was also achieved by the authors of the work (Ma et al., 2019) by examining the magnetite microspheres.
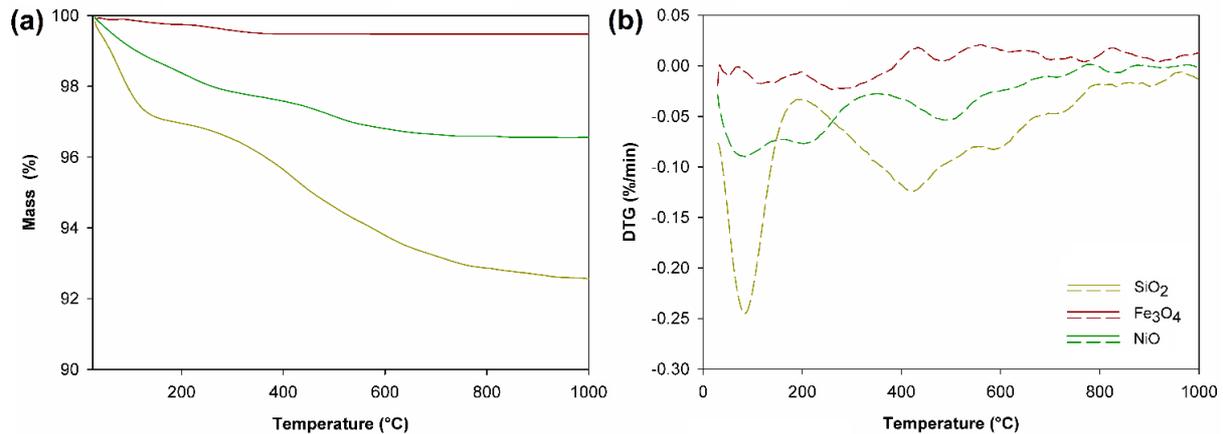
Fig. 3. Thermogravimetric (TGA) (a) and DTG (b) curves of oxide admixtures

3.2.   Cement composites analysis

3.2.1. Density

The measurements of the masses of samples allowed determining the density of the obtained cement mortars. Based on these results, it can be seen that pure mortar is characterized by the lack of significant changes in density and, moreover, shows the relatively highest density. Samples with the lowest density values contain admixtures of silicon dioxide. After 7 days, these samples are characterized by an average density value of 2.16 g/cm^3, and 2.20 g/cm^3 after 28 and 90 days, respectively. Cement composites containing admixtures of SiO_2+NiO and $SiO_2+Fe_3O_4$ oxide systems are characterized by the highest increases in average density. For the SiO_2+NiO interoxide system, a change was observed from 2.19 g/cm^3 after 7 days of maturation, to 2.25 g/cm^3 after 90 days. In the case of silica-magnetite cementitious composites, the values were 2.21 g/cm^3 and 2.27 g/cm^3, respectively. After 90 days of curing, the material containing an admixture of SiO_2 and Fe_3O_4 reached the density of the reference sample.

3.2.2. Water absorption

In the water absorption analysis, for each series, 5 samples were selected which, after 28 and 90 days of maturation in high humidity, were then placed in a dryer and dried to constant weight. The reference sample is pure cement mortar, containing no admixture, for which water absorption after 28 days of maturation was achieved at the level of 6.2%. A slightly lower value of water absorption, at the level of 6.0%, was achieved by samples of mortars doped with SiO_2+NiO oxide systems, while a value of 6.4% was achieved both by the mortars containing the SiO_2 admixture and the $SiO_2+Fe_3O_4$ oxide system. The analysis results indicate that the obtained absorbability results fully correspond to the cement mortar density. As hydration and bonding of the cementitious binder with the oxides proceed, the composite structure thickens and obtains better performance.

Table 2 presents also water absorption results after 90 days of maturation. After a longer maturation time, cement composites show lower water absorption. For the reference sample, a value of 2.5% was

reached. The lowest value was achieved by the $SiO_2+Fe_3O_4$ doped sample of 2.4%, while the highest one containing SiO_2+NiO - 3.1%. The reduced water absorption is related to the sealing of the cement composite structure after a longer maturation period.

Table 1. Medium densities for samples after 7, 28 and 90 days of maturation

Curing time (days)	Sample	Medium density (g/cm³)
7	Pure cement	2.27
	SiO_2	2.16
	SiO_2+NiO	2.19
	$SiO_2+Fe_3O_4$	2.21
28	Pure cement	2.27
	SiO_2	2.20
	SiO_2+NiO	2.21
	$SiO_2+Fe_3O_4$	2.23
90	Pure cement	2.27
	SiO_2	2.20
	SiO_2+NiO	2.25
	$SiO_2+Fe_3O_4$	2.27

Table 2. Water absorption results for samples after 28 and 90 days of maturation

Sample	Water absorption (%) After 28 days					Average	Water absorption (%) After 90 days					Average
	1	2	3	4	5		1	2	3	4	5	
Pure cement	6.2	6.4	6.2	6.1	6.0	**6.2±0.2**	2.5	2.2	2.1	2.5	2.9	**2.5±0.3**
SiO_2	6.5	6.6	6.1	6.3	6.3	**6.4±0.3**	2.8	2.6	2.5	3.2	3.5	**2.9±0.4**
SiO_2+NiO	6.1	6.0	5.9	6.0	6.0	**6.0±0.1**	3.4	2.3	3.2	3.4	3.0	**3.1±0.4**
$SiO_2+Fe_3O_4$	6.5	6.5	6.3	6.3	6.2	**6.4±0.2**	2.4	2.2	2.6	2.2	2.4	**2.4±0.2**

3.2.3. Compressive strength test results

Compressive strength was tested on samples of cement mortars after 7, 28 and 90 days of curing (see Fig. 4). All samples of cement composites doped with nanooxides reached compressive strengths higher than the reference sample. Mortars for which the highest compressive strength values were achieved contained admixtures of $SiO_2+Fe_3O_4$ binary oxide system. The highest values of compressive strength were observed after 7, 28 and 90 days of curing. The lowest compressive strength values among the doped samples were achieved by mortars containing only SiO_2 admixture, nevertheless, they were still significantly higher than the values obtained for pure mortar. The achieved strength values confirm the beneficial effect of SiO_2 admixture on the mechanical properties of the cement matrix. This outcome was also demonstrated in work by Zuang and Chen (Zhuang and Chen, 2019). The literature study carried out by the authors reveals that the SiO_2 admixture after 28 days of curing of the cement composite increases its strength in the range of 12-17% in relation to the reference sample.

In the case of the analyzed samples of mortars doped with the SiO_2+NiO system, an increase in strength was observed in relation to the mortar containing only SiO_2. This demonstrates the beneficial effect of adding NiO to cement mortars that comes about in the form of increasing compressive strength. Such outcome was also confirmed by Selim et al. (Selim et al., 2020), who performed compressive strength tests for cement mortars consisting of 80% OPC, 20% fly ash and admixtures of various miscellaneous nanoparticles that were subjected to elevated temperatures after maturation. For comparison, the strength was determined for pure mortar without nanoparticles admixture and mortars not exposed to high temperatures. Selim et al. used nanoparticles such as nano-Fe_2O_3 and nano-NiO as admixtures. The experimental data they obtained reveals the beneficial effect of the nanomaterials used.
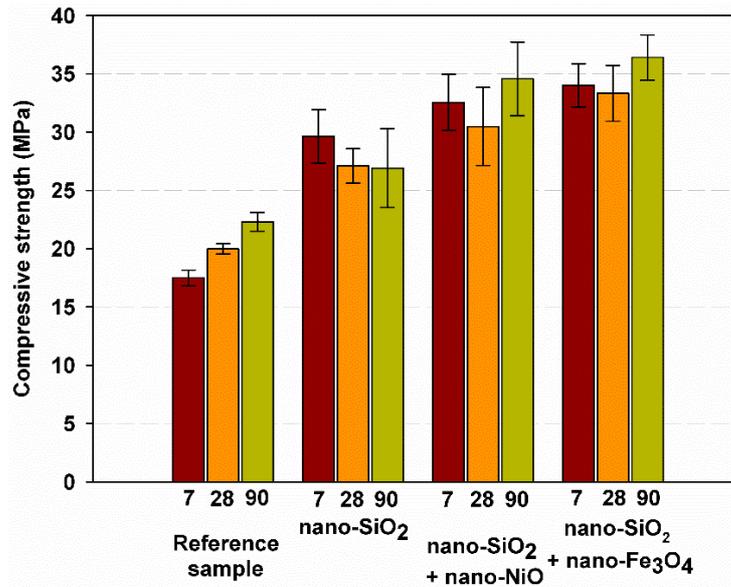
Fig. 4. Compressive strength analysis of cement mortars with nano-SiO_2 and interoxide systems of nano-SiO_2+nano-NiO and nano-SiO_2+nano-Fe_3O_4 after 7, 28 and 90 days of maturation

The additional increase in compressive strength, for binary oxide systems indicates that nickel nanooxide, as well as magnetite, represent, like nanosilica, additional active centers from which the growth of the C-S-H phase starts. This results in a gradual thickening of the composite microstructure and a build-up of strength, which is particularly evident during longer periods of cement binder curing. Unfortunately, this effect is not visible for the composite with silica, for which a spectacular increase in compressive strength occurs during the first 7 days of setting, and then these increases are not so pronounced. Nanosilica in the first days of cement binder setting fills the pores in the formed gel of the C-S-H phase, thus tightening the structure of the cement matrix and increasing the adhesion of the binder to the aggregate. Hence, in the first 7 days of setting, the cement matrix shows a significant increase in strength. At a later stage, however, the pozzolanic reaction becomes more important, during which the nanosilica reacts with calcium hydroxide formed during hydration of silicate phases of cement. As a result of this reaction, an additional C-S-H phase of much finer dimensions is formed, leading to an increase in the strength of the cement matrix after 28 and 90 days, compared to pure mortar. In contrast, nickel and magnetite nano-oxides, like other nano-oxides introduced into the cement matrix, e. g. titanium, zinc, aluminium, do not exhibit a pozzolanic reaction. They only act to densify the structure of the cement matrix by introducing additional active centres, from which the growth of the C-S-H phase begins. This resulted in additional increases in strength throughout the adolescence studied (Sobolev, 2016; Otulu and Sahin, 2011; Ren et al., 2018; Senff et al., 2012). The beneficial combination of nanosilica with other nanooxides may contribute to higher performance of cement composites over longer periods of time.

3.2.4. Microstructural analysis results

On the basis of the SEM images, in a sample of pure cement mortar (Fig. 5 a and a'), characteristic portlandite crystals, fibrillar C-S-H forms (Cerro-Prada et al., 2015) and ettryngite structures (Li et al., 2004) were observed. By comparing the microstructure of the pure mortar with the sample containing the SiO_2 admixture (Fig. 5 b, b'), the significant effect of the addition of nanoparticles on the cement matrix can be observed. Mortar with admixture is characterized by a more compact structure with smaller crystals and pores. This leads to compactness of microstructure and increase of compressive strength of composite.

The beneficial effect of silicon dioxide admixture was also demonstrated by (Zhuang and Chen, 2019), where, by comparing the structure of control group concrete with silica modified concrete, the sealing character of the admixture was demonstrated. Herein, the mortar containing nanooxide was characterized by a smaller size of pores and crystals, and the bonds between the crystals were shortened.
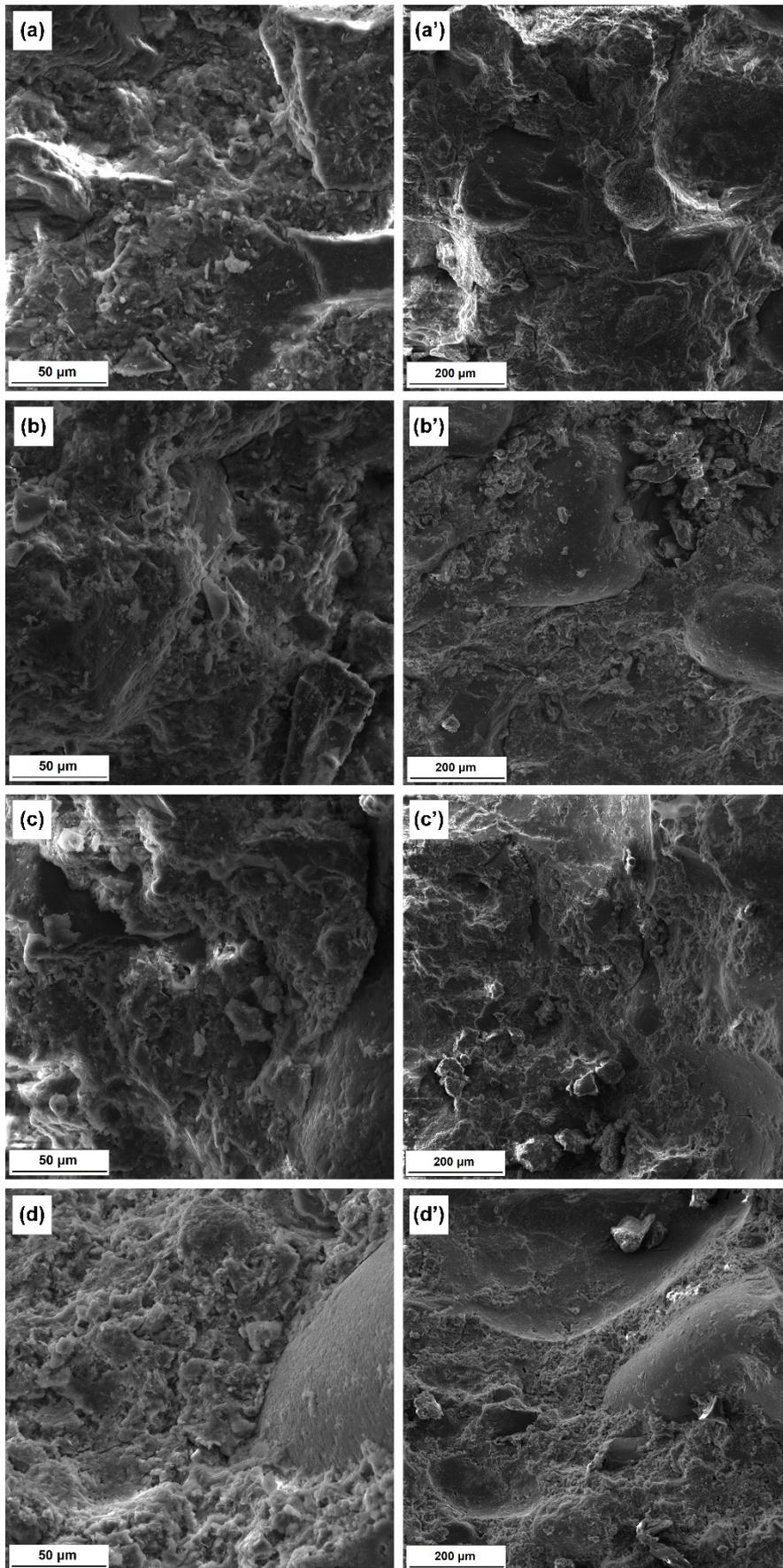
Fig. 5. SEM images of pure cement composite (a, a') and cement composites doped with SiO_2 (b, b'), SiO_2 with NiO (c, c') and SiO_2 with Fe_3O_4 (d, d')

In the case of cement mortars containing binary oxides - SiO_2 and Fe_3O_4, in the SEM images (see Fig. 5 d, d'), larger particles are clearly present in the microstructure of the cement composite, indicating the presence of magnetite. A similar effect on cement microstructure was obtained by Bowen et al. (Bowen et al., 2017). In their work, they included SEM images in which it was possible to observe clearly visible larger particles, unevenly distributed in the cement matrix, which were also related to the presence of magnetite. Due to the relatively large Fe_3O_4 particles, the microstructure of the cement sample is not as homogeneous as in the case of samples containing SiO_2 admixture and SiO_2+NiO system. When analyzing SEM images of mortars doped with SiO_2 and NiO (Fig. 5 c, c'), a similarly compact structure can be observed as in the case of SiO_2 admixture used alone.

4. Conclusions

As a result of the research, functional cement composites with the use of silicon dioxide nanoparticles and binary oxide systems SiO_2+NiO and $SiO_2+Fe_3O_4$ were obtained.

Based on the physicochemical analysis, the magnetite sample was confirmed to have the largest particles, and the NiO and SiO_2 samples - the smallest. All admixtures showed a tendency to aggregate and agglomerate. Still, the particles used differ in the properties of the porous structure. The silicon dioxide sample has the highest BET surface area (142.7 m^2/g) and pore volume (0.910 cm^3/g), while magnetite possessed the smallest (8.3 m^2/g and 0.025 cm^3/g, respectively). Moreover, the NiO sample was characterized by the lowest value of the mean pore size (6.3 m^2/g). As a result of the zeta potential analysis, the electrokinetic stability of the analyzed oxide samples was found to be in the range of -41.0-2.8 mV. Here, the SiO_2 and Fe_3O_4 curves are characterized by electrokinetic stability in a wider range compared to nickel oxide, however, the NiO sample alone reached the isoelectric point at pH equal to 1.8. The obtained electrokinetic stability fully enables the acceptability of using the above-mentioned oxides as admixtures for cement mortars characterized by a highly alkaline pH environment. The obtained thermogravimetric curves confirm the high thermal stability of the nanooxides used. The SiO_2 sample showed the highest weight loss (approx. 7%).

Finally, the analyzed materials, when used as admixtures for cement mortars, allowed a slight reduction in the density of cement mortars (2.27 g/cm^3 for pure mortar). In addition, the conducted water absorption analysis showed that the samples of mortars containing SiO_2 admixture and the binary oxide system $SiO_2+Fe_3O_4$ are characterized by slightly higher water absorption compared to the reference sample, while the SiO_2+NiO system is lower. The beneficial effect of the applied oxides on the compressive strength was revealed in mechanical tests carried out after 7, 28 and 90 days of curing. Here, the binary oxide system $SiO_2+Fe_3O_4$ sample was characterized by the highest strength values, while the lowest values were indicated for mortar containing only SiO_2 admixture. On the other hand, the microstructural analysis confirmed the sealing nature of the nanoparticles used.

References

BAGWE, R.P., HILLIARD, L.R., TAN, W., 2006. *Surface modification of silica nanoparticles to reduce aggregation and non-specific binding,* Langmuir, 22, 4357-4362.

BOWEN, G., DING, D., WANG, L., WU, J., XIONG, R., 2017. *The electromagnetic wave absorbing properties of cement-based composites using natural magnetite powders as absorber,* Mater. Res. Express, 4, 056103.

CERRO-PRADA, E., MANSO, M., TORRES, V., SORIANO, J., 2015. *Microstructural and photocatalytic characterization of cement-paste sol-gel synthesized titanium dioxide,* Front. Struct. Civ. Eng., 10, 189-197.

DORCHEH, A.S., ABBASI, M.H., 2008. *Silica aerogel; synthesis, properties and characterization,* J. Mater. Process. Technol. 199, 10-26.

HASAN, K., SHEHADI, I.A., AL-BAB, N.D., ELGAMOUZ, A., 2019. *Magnetic chitosan-supported silver nanoparticles: a heterogeneous catalyst for the reduction of 4-nitrophenol,* Catalysts, 9, 839.

JANCZAREK, M., KLAPISZEWSKI, Ł., JĘDRZEJCZAK, P., KLAPISZEWSKA, I., ŚLOSARCZYK, A., JESIONOWSKI, T., 2021. *Progress of functionalized TiO₂-based nanomaterials in the construction industry: A comprehensive review,* Chem. Eng. J. doi: 10.1016/j.cej.2021.132062.

KAMADA, K., TOKUTOMI, M., ENOMOTO, N., HOJO, J., 2005. *Incorporation of oxide nanoparticles into barrier-type alumina film via anodic oxidation combined with electrophoretic deposition*, J. Mater. Chem., 15, 3388–3394.

KLAPISZEWSKI, Ł., BULA, K., SOBCZAK, M., JESIONOWSKI, T., 2016. *Influence of processing conditions on the thermal stability and mechanical properties of PP/Silica-Lignin composites*, Int. J. Polym. Sci., Article ID 1627258.

KLAPISZEWSKI, Ł., KRÓLAK, M., JESIONOWSKI, T., 2014. *Silica synthesis by the sol-gel method and its use in the preparation of multifunctional biocomposites,* Centr. Eur. J. Chem., 12, 173-184.

KRYSZTAFKIEWICZ, A., RAGER, B., JESIONOWSKI, T., 1997. *The effect of surface modification on physicochemical properties of precipitated silica*, J. Mater. Sci., 32, 1333-1339.

LI, H., XIAO, H., YUAN, J., OU, J., 2004. *Microstructure of cement mortar with nano-particles*, Compos. B. Eng., 35, 185-189.

MA, M., YANG, Y., LI, W., FENG, R., LI, Z., LYU, P., MA, Y., 2019. *Gold nanoparticles supported by amino groups on the surface of magnetite microspheres for the catalytic reduction of 4-nitrophenol*, J. Mater. Sci., 54, 323-334.

NAZARI, A., RAFIEIPOUR, M.H., RIAHI, S., 2011. *The Effects of CuO Nanoparticles on Properties of Self Compacting Concrete with GGBFS as Binder*. Mat. Res., 14, 307-316.

NEGAHDARY, M., HABIBI-TAMIJANI, A., ASADI, A., AYATI, S., 2013. *Synthesis of Zirconia Nanoparticles and Their Ameliorative Roles as Additives Concrete Structures*, J. Chem. 2013, 314862.

OTULU, M., ŞAHIN, R., 2011, *Single and combined effects of nano-SiO₂, nano-Al₂O₃ and nano-Fe₂O₃ powders on compressive strength and capillary permeability of cement mortar containing silica fume*, Mater. Sci. Eng., A. 528, 7012–7019.

REN, J., LAI, Y., GAO, J., 2018. *Exploring the influence of SiO₂ and TiO₂ nanoparticles on the mechanical properties of concrete,* Constr. Build. Mater., 175, 277-285.

SANCHEZ, F., SOBOLEV, C., 2010. *Nanotechnology in concrete: A review*, Constr. Build. Mat., 24, 2060–2071.

SELIM, F.A., AMIN, M.S., RAMADAN, M., HAZEM, M.M., 2020. *Effect of elevated temperature and cooling regimes on the compressive strength, microstructure and radiation attenuation of fly ash-cement composites modified with miscellaneous nanoparticles*, Constr. Build. Mater., 258, 119648.

SENFF, L., HOTZA, D., LUCAS, S., FERREIRA, V.M., LABRINCHA, J.A., 2012. *Effect of nano-SiO₂ and nano-TiO₂ addition on the rheological behavior and the hardened properties of cement mortars,* Mater. Sci. Eng., 532, 354-361.

SOBOLEV, K., 2016. *Modern developments related to nanotechnology and nanoengineering of concrete*, Front. Struct. Civ. Eng., 10(2), 131–141.

SONG, X., JIANG, N., LI, Y., XU, D., QIU, G., 2008. *Synthesis of CeO₂-coated SiO₂ nanoparticle and dispersion stability of its suspension,* Mater. Chem. Phys., 110, 128-135.

ŚLOSARCZYK A., KWIECIŃSKA, A., PEŁSZYK, E., 2017. *Influence of selected metal oxides in micro and nanoscale on the mechanical and physical properties of the cement mortars.* Procedia Eng., 172, 1031-1038.

XAVIER, J.R., 2020. *Electrochemical, mechanical and adhesive properties of surface modified NiO-epoxy nanocomposite coatings on mild steel*, Mater. Sci. Eng. B, 260, 114639.

ZDARTA, J., SAŁEK, K., KOŁODZIEJCZAK-RADZIMSKA, A., SIWIŃSKA-STEFAŃSKA, K., SZWARC-RZEPKA, K., NORMAN, M., KLAPISZEWSKI, Ł., BARTCZAK, P., KACZOREK, E., JESIONOWSKI, T., 2015. *Immobilization of* Amano Lipase A *onto Stober silica surface: process characterization and kinetic studies,* Open Chem., 13, 138-148.

ZHAO, M., LI, N., ZHENG, L., LI, G., YU, L., 2008. *Synthesis of well-dispersed NiO nanoparticles with a room temperature ionic liquid*, J. Dispers. Sci. Technol., 29, 1103-1105.

ZHU, W., BARTOS, P., PORRO, A., 2004. *Application of nanotechnology in construction. Summary of a state-of-the-art report.* RILEM TC 197-NCM. Mater. Struct., 37, 649–658.

ZHUANG, C., CHEN, Y., 2019. *The effect of nano-SiO₂ on concrete properties: a review.* Nanotechnol. Rev., 8, 562-572.